Non-equilibrium Relaxation and Aging Scaling of the Coulomb and Bose Glass

Matthew T. Shimer[1,2], Uwe C. Täuber[1], and Michel Pleimling[1]
[1]*Department of Physics (MC 0435), Robeson Hall, 850 West Campus Drive, Virginia Tech, Blacksburg, VA 24061 and*
[2]*hMetrix LLC, 150 Monument Rd, # 107, Bala Cynwyd, PA 19004*
(Dated: August 29, 2014)

We employ Monte Carlo simulations to investigate the non-equilibrium relaxation properties of the two- and three-dimensional Coulomb glass with different long-range repulsive interactions. Specifically, we explore the aging scaling laws in the two-time density autocorrelation function. We find that in the time window and parameter range accessible to us, the scaling exponents are not universal, depending on the filling fraction and temperature: As either the temperature decreases or the filling fraction deviates more from half-filling, the exponents reflect markedly slower relaxation kinetics. In comparison with a repulsive Coulomb potential, appropriate for impurity states in strongly disordered semiconductors, we observe that for logarithmic interactions, the soft pseudo-gap in the density of states is considerably broader, and the dependence of the scaling exponents on external parameters is much weaker. The latter situation is relevant for flux creep in the disorder-dominated Bose glass phase of type-II superconductors subject to columnar pinning centers.

PACS numbers: 75.10.Nr 71.55.Jv, 05.70.Ln, 74.25.Uv

I. INTRODUCTION

The Coulomb glass model was devised to describe the physical properties of localized charge carriers in disordered semiconductors [1–3]. It assumes that the localization length ξ is small or of the order of the mean separation a_0 between acceptor or donor sites, whence the system can be essentially described in classical terms: Charged particles are confined to randomly distributed sites, and at low temperatures the system equilibrates through rearrangement of the carrier distribution to minimize the total interaction energy. In semiconductors, these variable-range hopping processes are effected through phonon-assisted tunneling between the acceptor / donor sites. The strong spatial (anti-)correlations resulting from the long-range repulsive forces in turn induce a marked depletion of the (interacting) single-particle density of states, i.e., the distribution function $g(\epsilon)$ of the site energies, near the chemical potential μ_c that separates low-energy ($\epsilon < \mu_c$) filled states from empty states at elevated energies ($\epsilon > \mu_c$). In the presence of this correlation-induced soft Coulomb gap, carrier mobility thus becomes considerably impeded [2]: If $g(\epsilon) \sim |\epsilon - \mu_c|^\gamma$ follows a power law in the vicinity of μ_c with an (effective) gap exponent γ, the associated conductivity scales as $\ln \sigma \sim -T^{-p}$, with $p(\gamma) = (\gamma+1)/(\gamma+d+1)$ in d spatial dimensions in the thermally activated transport regime at low temperatures T. Note that $p(\gamma) \geq 1/(d+1) = p(\gamma \to 0)$, the Mott variable-range hopping exponent applicable for a finite density of states $g(\mu_c) > 0$. Electron tunneling experiments in doped semiconductors have confirmed the existence of correlation-induced soft gaps in the density of states [4, 5].

The two-dimensional Coulomb glass model, with the electrostatic $1/r$ potential essentially replaced by a logarithmic repulsion, has furthermore been adapted to capture the static properties as well as thermally activated flux creep in type-II superconductors with extended, linear disorder aligned along the magnetic-field direction [6]. These columnar defects serve as effective pinning sites for fluctuating magnetic flux lines; at low temperatures T (and driving currents J) they undergo a continuous localization transition [7, 8]. In this localized Bose glass phase, the pinned flux lines are essentially straight and parallel, rendering the system effectively two-dimensional, and vortex transport between columnar defects proceeds in analogy to variable-range hopping through formation and subsequent relaxation of double kinks between different pinning sites [9, 10]. Long-range repulsive vortex interactions again induce a soft gap in the density of states which strongly suppresses flux creep, leading to a desired much reduced resistivity $\ln \rho \sim -J^{-p}/T$ [11] (for magnetic flux densities smaller than the matching field, at which the number of flux lines equals the number of columnar defects; for extensions to the regime near and beyond the matching field, see Refs. [12, 13]).

Over the past three decades, intense research into the correlation-dominated equilibrium features [14–26] as well as non-equilibrium relaxation properties [27–41] of the Coulomb glass have considerably advanced our understanding of this paradigmatic model system for highly correlated disordered materials. In part motivated by the unambiguous experimental confirmation of aging effects in relaxation measurements for the conductivity of a two-dimensional silicon sample, and scaling near its metal-insulator transition [42, 43], in this work we focus on a numerical study of the non-equilibrium relaxation properties of the Coulomb glass following a quench from a fully uncorrelated, high-temperature initial state.

Although the soft Coulomb gap in the site energy distribution forms quite fast, subsequent relaxation towards the equilibrium terminal state is sufficiently slow to open a sufficiently wide time window wherein time translation

invariance is broken and aging scaling is clearly observed (for recent overviews on non-equilibrium relaxation and aging phenomena, see Refs. [44, 45]). Specifically, we employ a variant of the Monte Carlo algorithm described in Refs. [31, 32] to investigate the dependence of the ensuing aging scaling exponents for various Coulomb glass systems as function of temperature T, filling fraction (total charge carrier density) K, dimensionality, and form of the repulsive interaction potential (Coulomb $1/r$ potential in $d = 2, 3$ dimensions; logarithmic potential in two dimensions). A first, concise account of aging in the two-dimensional Coulomb case was presented in Ref. [37]; we note that further technical details and additional data can be found in Ref. [46].

In the following Sec. II, we introduce our model Hamiltonian and explain our Monte Carlo simulation algorithm. We also briefly discuss basic simulation results pertaining to the emerging Coulomb gap in the (interacting) single-particle density of states. Section III addresses non-equilibrium relaxation properties of our system as obtained from measurements of the two-time density autocorrelation function, starting from random initial conditions. The obtained aging scaling exponents and their dependence on temperature, filling fraction, interaction potential, and dimensionality constitute the central findings of this work. We conclude with a brief summary and discussion.

II. MODEL DESCRIPTION AND MONTE CARLO SIMULATIONS

In this section, we briefly describe the Coulomb glass model, explain our Monte Carlo algorithm, and list our results on equilibrium properties obtained from our simulation runs in two and three dimensions with different interaction potentials.

A. The Coulomb Glass Model

The Coulomb glass model was introduced by Efros and Shklovskii to capture thermodynamic and transport properties of localized charge carriers in doped semiconductors [1]. A set of multiple, randomly (Poisson) distributed but fixed localized pinning sites (here selected off-lattice on a continuum) are available to the charge carriers in d spatial dimensions. Because of the strong intra-site correlations these sites labeled by an index i can only contain at most a single particle, which restricts the site occupation numbers to $n_i = 0, 1$. The system is dominated by long-range repulsive interactions $V(r)$ between the charge carriers. The combination of quenched spatial site disorder and long-range interactions induce strong correlation effects.

For the case of unscreened Coulomb interactions, the Hamiltonian of the Coulomb glass model reads [1, 2]

$$H(\{n_i\}) = \sum_i n_i \varphi_i + \frac{e^2}{2\kappa} \sum_{i \neq j} \frac{(n_i - K)(n_j - K)}{|\mathbf{R}_i - \mathbf{R}_j|}, \quad (1)$$

where e denotes the carrier charge, κ a dielectric constant, and $\mathbf{R}_i$, φ_i, and n_i respectively represent the position vector, (bare) site energy, and occupancy of the ith site, $i = 1, \ldots, N$. The first term corresponds to (random) site energies assigned to each accessible location; since the system is dominated by the long-range forces, we choose all $\varphi_i = 0$ to further simplify the model, while drawing the positions $\mathbf{R}_i$ at random from a two- or three-dimensional continuous set [18, 28, 31, 32]. The second contribution encapsulates the repulsive Coulomb interactions (with dielectric constant κ). In order to maintain global charge neutrality, a uniform relative charge density $K = \sum_i n_i/N$ is inserted; it constitutes the total carrier density per site or filling fraction. Note that with $\varphi_i = 0$ the Hamiltonian (1) displays particle-hole symmetry, i.e., systems with filling fractions $K = 0.5+k$ and $K = 0.5-k$ are equivalent. Upon replacing the site occupation numbers with Ising spin variables $\sigma_i = 2n_i - 1 = \mp 1$, the Coulomb glass maps onto a random-site, random-field antiferromagnetic Ising model with long-range exchange interactions [14].

The Coulomb glass model may be adapted to describe the low-temperature properties of magnetic flux lines in type-II superconductors with strong columnar pinning centers [9–11]. Deep in the Bose glass phase, the vortices become localized at the linear material defects, and thermal transverse wandering is strongly suppressed, which renders the system essentially two-dimensional. The mutual repulsion interaction between two occupied sites is now characterized by a modified Bessel function $K_0(r/\lambda)$, essentially a long-range logarithmic potential that is screened on the scale of the London penetration depth λ, and the Hamiltonian becomes

$$H(\{n_i\}) = \epsilon_0 \sum_{i \neq j} (n_i - K)(n_j - K)\, K_0\left(\frac{|\mathbf{R}_i - \mathbf{R}_j|}{\lambda}\right). \quad (2)$$

The energy scale is now set by $\epsilon_0 = (\phi_0/4\pi\lambda)^2$ with the magnetic flux quantum $\phi_0 = hc/2e$. We shall address the dilute low-magnetic field regime where all site distances $r_{ij} = |\mathbf{R}_i - \mathbf{R}_j| \ll \lambda$ and thus $K_0(x) \approx -\ln x$ (aside from a constant). The random site positions $\mathbf{R}_i$ are drawn from a continuous flat distribution in two dimensions.

B. Monte Carlo Simulation Algorithm

The Monte Carlo simulations were initiated by randomly placing N sites within a square in two / cube in three dimensions. Initially, we prepared the system in a completely uncorrelated configuration, distributing KN charge carriers at random among the N available sites. The "charged" particles may then attempt hops

from occupied sites a (with $n_a = 1$) to unoccupied sites b ($n_b = 0$). Following Refs. [31, 32], two multiplicative factors determine the success rate of this hop, namely (i) a strongly distance-dependent transfer process that respectively models phonon-mediated tunneling in semiconductors, and vortex superkink proliferation in type-II superconductors, and (ii) thermally activated jumps over energy barriers represented by a Metropolis factor:

$$\Gamma_{a\to b} = \tau_0^{-1}\, e^{-2r_{ab}/\xi}\, \min[1, e^{-\Delta E_{ab}/T}]\,, \qquad (3)$$

where τ_0 represents a microscopic time scale, $r_{ij} = |\mathbf{R}_i - \mathbf{R}_j|$ is the distance between sites i and j, while ξ characterizes the spatial extension of the localized carrier wave functions / thermal wandering of the magnetic flux lines (we set Boltzmann's constant $k_{\rm B} = 1$). The rate for a thermally activated move from occupied site a to empty site b is determined by the energy difference $\Delta E_{ab} = \epsilon_b - \epsilon_a - V(r_{ab})$, with the (interacting) site energies $\epsilon_i = \sum_{j\neq i}(n_j - K)\, V(r_{ij})$, and where the long-ranged interactions are governed by the Coulomb potential $V(r) = e^2/\kappa r$ for semiconductor charge carriers, whereas $V(r) = 2\epsilon_0\, K_0(r/\lambda)$ for magnetic vortices.

The simulation consecutively performs the following four stochastic processes [37, 46]: (i) Randomly select an occupied site a ($n_a = 1$). (ii) Choose an unoccupied site b ($n_b = 0$) from the exponential probability distribution in the first, "tunneling" term in Eq. (3). (iii) Attempt a hop with a success probability determined by the Metropolis factor in Eq. (3). (iv) If the hop attempt fails, return to step one. If it is successful, move the particle from site a to site b. Each Monte Carlo time step (MCS) consists of N iterations of (i)–(iv). Note that all pair potential values $V(r_{ab})$ may be calculated at the beginning of the simulation run. Subsequently, only the site energies of sites a and b need to be evaluated, which merely requires a summation of the pre-calculated pair potentials. Collecting these interacting site energies and averaging over many independent realizations with different random site placements, we then compiled the (interacting) single-particle density of states $g(\epsilon)$, to be discussed in the following subsection. With all occupation numbers n_i recorded at each time step, we could furthermore study the temporal evolution of the two-time carrier density autocorrelation function, see Sec. III.

In the following, distances are measured relative to the mean separation a_0 between sites, and energies as well as temperature scales are given in units of the typical energy scales $e^2/\kappa a_0$ and $2\epsilon_0\, K_0(a_0/\lambda)$, where we used $\lambda/a_0 = 8$. As in Refs. [31, 32], we set $\xi = a_0$; we have in fact explored other values for ξ as well, $0.5a_0$ and $2a_0$, but (within the applicability range of the model) found that the ensuing changes can simply be absorbed into a renormalized overall time scale τ_0. Initially, KN particles were placed at random on the $N = L^d$ available sites to mimic a quench from a very high temperature. Then the system was evolved for typically 10^6 MCS at temperature T with the Monte Carlo dynamics defined by the generalized Metropolis rate (3). We employed periodic boundary conditions, whence the potential due to charges outside the simulation cell was calculated by mirroring it on the $2d$ adjacent faces. The minimum of the distances between any given sites i and j and the latter's $2d$ mirror images in neighboring cells is used to compute the interaction potential $V(r_{ij})$.

We performed simulations for different system sizes $8 \leq L \leq 32$; with temperatures in the range $0.001 \leq T \leq 0.1$; and filling fractions in the interval $0.25 \leq K \leq 0.5$ (equivalent to $0.5 \leq K \leq 0.75$ due to particle-hole symmetry). Running the simulations with various system sizes L, we noticed no measurable finite-size effects; for example, deviations between the obtained density autocorrelations at $L = 10$ and $L = 16$ were less than 2% [46]. For each configuration (temperature T, filling fraction K, etc.), the data were averaged over at least 1000 independent simulation runs. Temperatures larger than 0.03 turned out not to be useful for our study of aging processes since equilibrium was then reached far too quickly. In contrast, for $T < 0.01$, the kinetics slowed down too much for gathering statistically significant data within computationally reasonable time frames. As will be discussed in more detail below, the dynamics also freezes out within the numerically accessible simulation times for filling fractions $K < 0.4$ (or $K > 0.6$).

C. Coulomb Gap Properties

The long-range interactions quickly generate strong correlations among the "charged" particles. As they maximize their distances subject to the availability of randomly placed pinning sites, in equilibrium a pronounced soft Coulomb gap forms at zero temperature in the (interacting) single-particle density of states, or distribution of site energies $g(\epsilon)$ [2]. Following Efros and Shklovskii's insightful mean-field argument, this interacting density of states vanishes precisely at the chemical potential μ_c that separates the low-energy filled sites from the more energetic empty sites, $g(\mu_c) = 0$. For a power-law repulsive interaction potential $V(r) \sim r^{-\sigma}$, the mean-field analysis further predicts that for $\sigma < d$

$$g(\epsilon) \sim |\epsilon - \mu_c|^{\gamma} \qquad (4)$$

vanishes algebraically near μ_c in d dimensions, with the positive gap exponent $\gamma = (d/\sigma) - 1$ [2, 11]. Beyond mean-field theory, this expression still represents a lower bound for γ [26]. Indeed, Monte Carlo simulations typically yield gap exponent values that exceed the mean-field estimate [11, 14, 16, 17, 19], especially in the absence of random on-site disorder ($\varphi_i = 0$). For example, in their very detailed numerical Coulomb glass study with up to $N = 125,000$ and $40,000$ sites in $d = 3$ and $d = 2$ dimensions, Möbius and Richter measured $\gamma = 2.6 \pm 0.2$ and $\gamma = 1.2 \pm 0.1$, respectively [19]. More recent studies, however, found gap exponents much closer to the mean-field predictions [24, 25]. Tunneling experiments on the non-metallic semiconductor Si:B samples yielded a gap

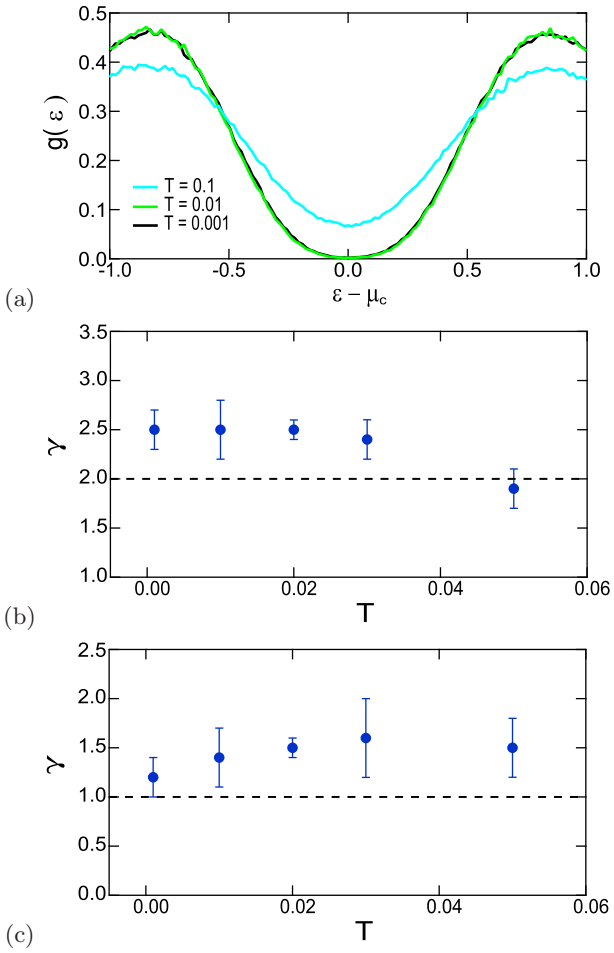

FIG. 1: (Color online) (a) Density of states $g(\epsilon)$ for the three-dimensional Coulomb glass ($L = 8$, $N = 512$ sites) at half-filling $K = 0.5$, at temperatures $T = 0.001$ (black), $T = 0.01$ (green/gray), and $T = 0.1$ (light blue/light gray). (b) Corresponding (effective) gap exponents $\gamma(T)$ vs. temperature; (c) gap exponent $\gamma(T)$ in two dimensions ($L = 16$, $N = 256$, $K = 0.5$). The dashed lines represent the mean-field prediction $\gamma = d - 1$.

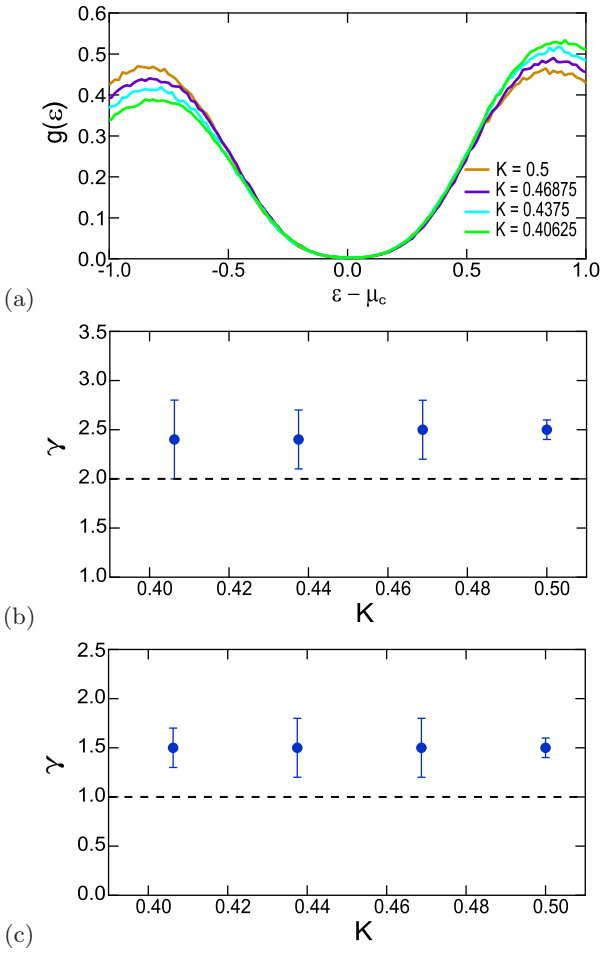

FIG. 2: (Color online) (a) Coulomb glass density of states $g(\epsilon)$ in three dimensions ($L = 8$, $N = 512$ sites) at temperature $T = 0.02$, for various filling fractions $K = 0.5, 0.46875, 0.4375$, and 0.40625 (from bottom to top on right). (b) Corresponding (effective) gap exponents $\gamma(K)$ vs. filling fraction; (c) gap exponent $\gamma(K)$ in two dimensions ($L = 16$, $N = 256$, $T = 0.02$); the dashed lines show the mean-field values $\gamma = d - 1$.

exponent $\gamma \approx 2.2$ [4], while transport measurements on ultrathin Be films were compatible with the mean-field value $p = 1/2$, i.e., $\gamma = 1$ for $d = 2$ [5]. For the two-dimensional Bose glass with essentially logarithmic repulsion, the mean-field argument predicts an exponential gap ($\sigma \to 0$); in contrast, the data in Ref. [11] from zero-temperature simulations with $N = 400$ sites could best be fitted with power laws and (perhaps just effective) gap exponents that increase with decreasing filling fraction K, ranging from $\gamma \approx 2.2$ for $K = 0.4$ to $\gamma \approx 2.9$ for $K = 0.1$. Indeed, correlation effects should be strongest far away from half-filling, since the charged particles are then least affected by the Poissonian spatial disorder.

In our Monte Carlo simulations performed in the absence of a background random site energy distribution, the Coulomb gap in the single-particle density of states forms very quickly, and appears fully formed within $\sim 50 \ldots 100$ MCS [37, 46]. To make contact with previous work, we have measured the interacting density of states / distribution of site energies, and obtained approximate values for the effective gap exponents γ from best linear fits near the chemical potential μ_c in double-logarithmic plots. In Fig. 1(a), we display results for the temperature dependence of the shape of $g(\epsilon)$ for the three-dimensional Coulomb glass with repulsive $1/r$ interaction potential at half-filling. The graphs for $T = 0.001$ and $T = 0.01$ are indistinguishable within the statistical errors. At elevated temperature $T = 0.1$, $g(\mu_c)$ attains a non-zero value; when the temperature scale reaches the width of the soft gap in the density of states, the Coulomb gap begins to fill owing to thermal excitations that wash out the sharp boundary between filled and empty energy levels. As shown in Fig. 1(b), the three-dimensional gap exponent $\gamma(T)$ becomes independent of T once thermal excitations can be neglected. In contrast, in two dimen-

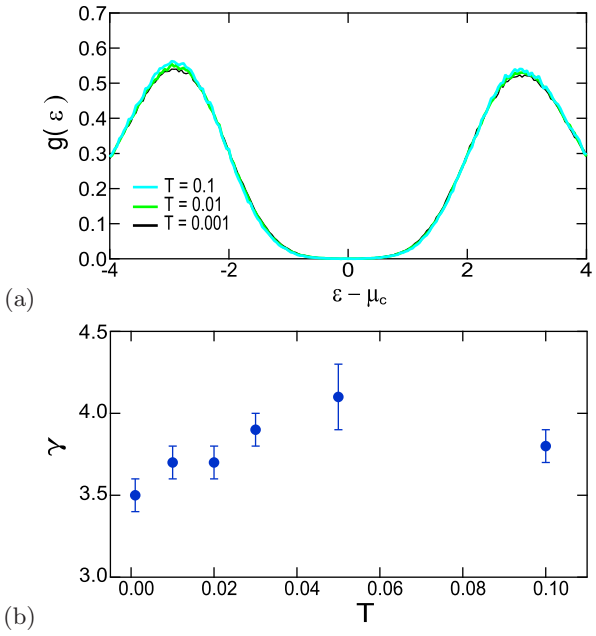

FIG. 3: (Color online) (a) Density of states $g(\epsilon)$ for the two-dimensional Bose glass ($L = 16$, $N = 256$ sites) for $K = 0.5$, at temperatures $T = 0.001$ (black), $T = 0.01$ (green/gray), and $T = 0.1$ (light blue/light gray). (b) Corresponding (effective) gap exponents $\gamma(T)$ vs. temperature.

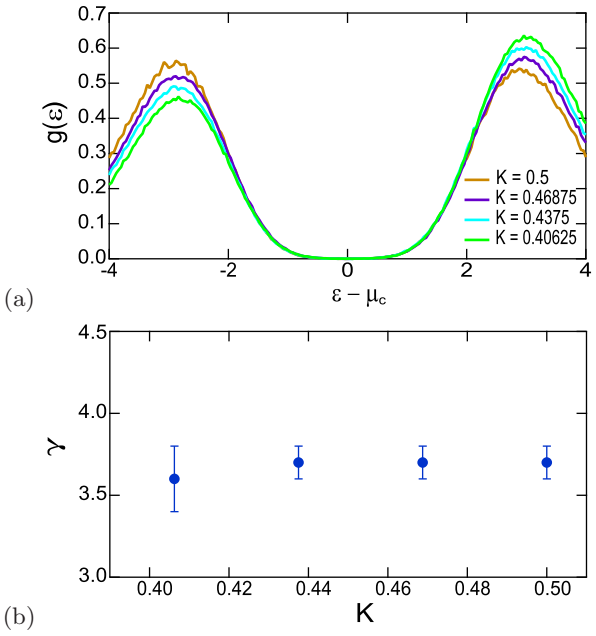

FIG. 4: (Color online) Bose glass density of states $g(\epsilon)$ in two dimensions ($L = 16$, $N = 256$ sites) at temperature $T = 0.02$, for filling fractions $K = 0.5, 0.46875, 0.4375$, and 0.40625 (from bottom to top on right). (b) Corresponding (effective) gap exponents $\gamma(K)$ vs. filling fraction.

sions, Fig. 1(c), we observe a stronger temperature dependence of the effective gap exponent. Extrapolating to $T \to 0$, our numerical values $\gamma \approx 2.5 \pm 0.2$ for $d = 3$ and $\gamma \approx 1.2 \pm 0.2$ deviate from the mean-field prediction $\gamma = d - 1$ (for $\sigma = 1$), and are in good agreement with Ref. [19]. The displayed error bars merely represent the statistical errors which vary with the number of independent realizations used for each parameter set.

In Fig. 2, we study the dependence of the soft Coulomb gap on the filling fraction K. Moving away from half-filling, $g(\epsilon)$ naturally becomes increasingly asymmetric. Yet near its minimum at μ_c, the curves in Fig. 2(a) collapse onto each other, resulting in gap exponents $\gamma(K)$ that are essentially independent of the total charge carrier density K, at least in the small range $0.4 < K \leq 0.5$.

Next we explore the distribution of site energies in the two-dimensional Bose glass with long-range, essentially logarithmic repulsion ($\lambda = 8a_0$). As is evident in Fig. 3(a), the emerging soft correlation gap is wider by a factor of 5 as compared to the data for the Coulomb $1/r$ interaction. Therefore, even at $T = 0.1$ no thermal effects can be visibly discerned. Yet measuring the effective gap exponent reveals an even steeper temperature dependence of $\gamma(T)$ than for the two-dimensional Coulomb glass, compare Fig. 3(b) with Fig. 1(c), extrapolating to $\gamma \approx 3.5 \pm 0.1$ as $T \to 0$ at half filling $K = 1/2$, a considerably larger value than reported in Ref. [11]; in that study, however, no neutralizing charge background was employed, i.e., K was set to zero in the Hamiltonian (2). As depicted in Fig. 4, the dependence of the effective gap exponent $\gamma(K)$ on the filling fraction K is rather weak within the interval $0.4 < K \leq 0.5$.

III. NON-EQUILIBRIUM RELAXATION AND AGING SCALING

We now proceed to our numerical results for non-equilibrium relaxation features of the Coulomb and Bose glasses initially prepared in a random, high-temperature state, as measured in the two-time density autocorrelation function. We first discuss the general relaxation scenario and the two distinct aging scaling fits we have implemented, before we provide the resulting scaling exponent values.

A. Two-Time Density Autocorrelation Function

In our initially entirely random distribution of charge carriers in the system, inevitably many particles are placed in close vicinity. They strongly repel each other and are fast displaced to energetically much more favorable sites. Correspondingly, the soft correlation-induced Coulomb gap in the density of states develops quite rapidly within $50 \ldots 100$ MCS. Subsequently subtle spatial rearrangements take place that further reduce the total energy, as becomes clearly visible in the temporal evolution of the energy landscape contour plots shown in Fig. 5. These processes proceed on considerably longer

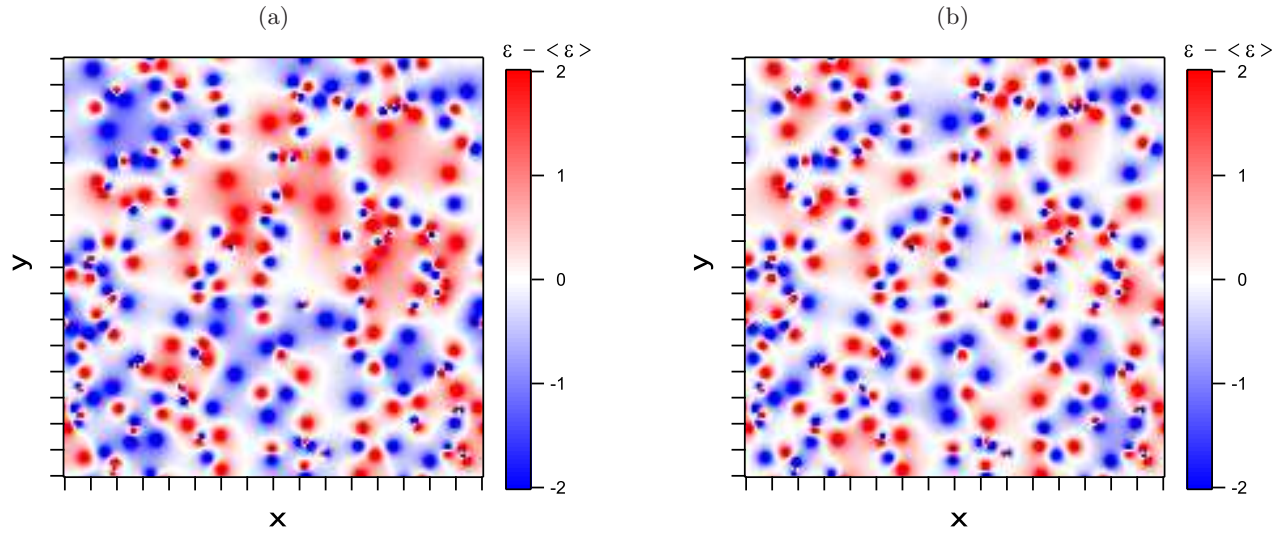

FIG. 5: Energy landscape contour plots for the Coulomb glass with $1/r$ potential in $d = 2$ dimensions ($L = 16$, $K = 1/2$, $T = 0.02$) after (a) 10 MCS and (b) 10^6 MCS.

time scales; yet in this intermediate regime the system retains memory of its initial configuration, and time translation invariance is broken, in contrast to the asymptotic stationary, equilibrated state [44, 45].

In order to monitor the slow structural relaxation kinetics in the Coulomb and Bose glass, we compute the (normalized) two-time carrier density autocorrelation function [31, 32, 37]

$$C(t,s) = \frac{\langle n_i(t) n_i(s)\rangle - K^2}{K(1-K)} = \frac{\sum_i n_i(t) n_i(s) - K^2 N}{K(1-K)N}\,, \tag{5}$$

where s indicates the elapsed time after the high-temperature quench, when the Monte Carlo simulation runs are initiated, while $t > s$ refers to a later "measurement time" when the temporal correlations are obtained relative to the "waiting time" s. Since $n_i^2 = n_i$ and $\sum_i n_i = KN$, at equal times $C(s,s) = 1$.

Representative data from our simulation runs are displayed in Fig. 6. The linear plot of $C(t,s)$ vs. the measurement time t in Fig. 6(a) shows that even after 10^6 MCS no stationary, equilibrium state has been reached yet. Graphing the same autocorrelation data against the time difference $t - s$, in Fig. 6(b) on a logarithmic scale, establishes that time translation invariance is indeed manifestly broken. In accord with the data of Ref. [31], we observe that following a fast initial decay towards an almost flat quasi-"plateau" region, the graphs for different waiting times s become distinct. Indeed, the longer "aged" runs for larger waiting times remain in an intermediate state for more extended time periods, before the density autocorrelation ultimately resumes its slower relaxation towards zero. In analogy with the phenomenology in structural glasses (see, e.g., Ref. [47]), we term these two distinct relaxation regimes visible in our data "β" and "α relaxation", respectively. In the following, we address the power law scaling for the slow density relaxation processes in the α relaxation regime.

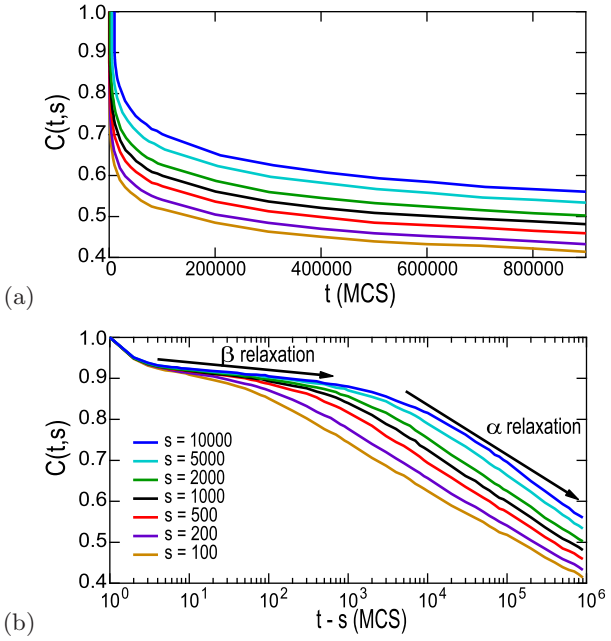

FIG. 6: (Color online) Non-equilibrium relaxation and aging for the carrier density autocorrelation function (5) in the two-dimensional Coulomb glass (for $L = 16$, $K = 1/2$, $T = 0.02$). (a) $C(t,s)$ vs. t for various waiting times $s = 100, 200, 500, 1000, 2000, 5000, 10000$ (from bottom to top); (b) same data plotted vs. $t - s$ on a logarithmic scale.

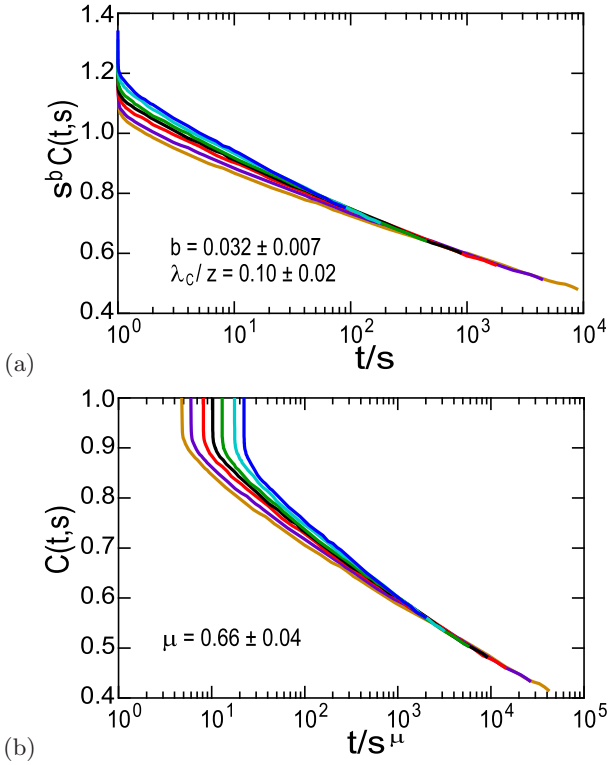

FIG. 7: (Color online) Aging scaling collapse for the density autocorrelation function (5) in the two-dimensional Coulomb glass (for $L = 16$, $K = 1/2$, and $T = 0.02$), obtained for the set of waiting times $s = 100, 200, 500, 1000, 2000, 5000, 10000$ (from bottom to top): (a) full aging scaling according to Eq. (6) with $\mu = 1$; (b) subaging scaling, Eq. (6) with $b = 0$.

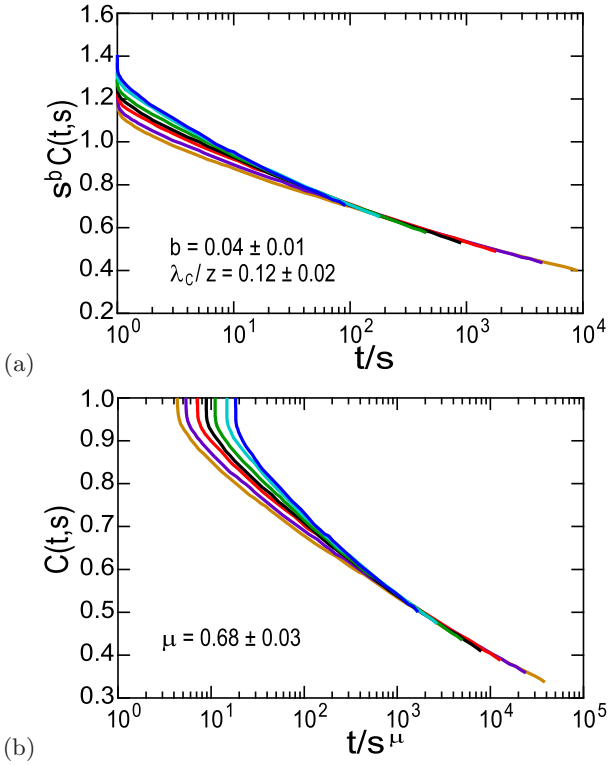

FIG. 8: (Color online) Aging scaling collapse for the density autocorrelations as in Fig. 7, but now for the three-dimensional Coulomb glass ($L = 8$, $K = 1/2$, and $T = 0.02$; waiting times s as in Figs. 6 and 7).

B. Dynamical Aging Scaling

We consider the aging scaling limit, where both $s, t \gg \tau_0$ (or any other microscopic time scale), and in addition $t \gg s$. i.e., $t - s \gg \tau_0$. In the α relaxation regime, time translation invariance does not hold, whence the carrier density two-time autocorrelation function (5) does not just depend on the time difference $t - s$, but on both t and s separately. Following the notations in Ref. [45], we posit the following general aging scaling form

$$C(t, s) = s^{-b} f_C(t/s^{\mu}) \,, \tag{6}$$

with scaling exponents $b \geq 0$ and $\mu \leq 1$. In many simple, analytically tractable situations, characterized by a single algebraically growing length scale $L(t) \sim t^{1/z}$ with dynamic scaling exponent $z \geq 1$, one in fact obtains aging scaling laws of the form (6) with $\mu = 1$, often referred to as "full aging". In the limit $t/s \to \infty$, in this situation one furthermore expects the scaling function to follow the algebraic decay

$$f_C(x) \sim [L(t)/L(s)]^{-\lambda_C} \sim (t/s)^{-\lambda_C/z} \tag{7}$$

with the autocorrelation exponent $\lambda_C \geq 0$. Prominent examples that display this full aging scaling scenario are the purely relaxational dynamics in the kinetic Ising model in one dimension [48, 49], time-dependent Ginzburg-Landau models quenched to the critical point [50, 51], and coarsening of the spherical model A in the low-temperature phase, both with short-range [52, 53] and long-range [54–56] interactions.

In Fig. 7(a), we demonstrate scaling collapse of the two-dimensional Coulomb glass density autocorrelation data from Fig. 6 ($L = 16$) utilizing the full-aging scaling form (6) with $\mu = 1$. Focusing on the data for $t - s$ in the range $3 \cdot 10^4 \ldots 10^6$ MCS, and following the interpolation method described in Ref. [57], we obtain optimal collapse onto a single master curve for $b = 0.032 \pm 0.007$. From the asymptotic long-time decay we furthermore infer $\lambda_C/z \approx 0.10 \pm 0.02$ for $T = 0.02$ at half filling $K = 1/2$ [37].

Alternatively, one may impose $b = 0$ in Eq. (6), and instead work with a non-trivial scaling exponent $\mu < 1$; this "subaging scaling" is frequently employed in the spin glass literature [45]. As purely phenomenological fits, both scaling ansätze are in essence equivalent. The subaging scaling collapse of our data for the two-dimensional Coulomb glass is depicted in Fig. 7(b), best fit with the value $\mu = 0.66 \pm 0.04$ [37]. Similar scaling properties are obtained for the three-dimensional Coulomb glass as well as for the two-dimensional Bose Glass. Figs. 8 and 9 show a characteristic example for each of these two cases.

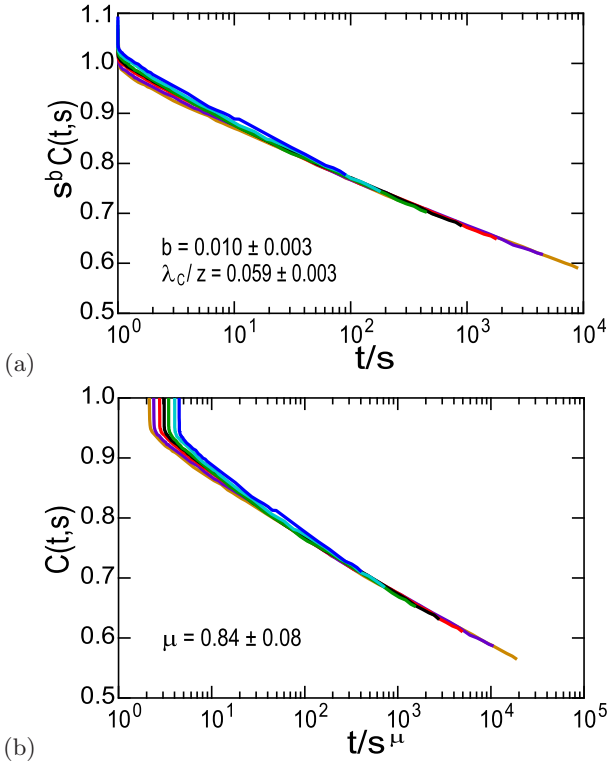

FIG. 9: (Color online) Aging scaling collapse for the density autocorrelations as in Fig. 7, for the two-dimensional Bose glass with $L = 24$, $K = 1/2$, and $T = 0.02$; waiting times s as in Figs. 6 and 7.

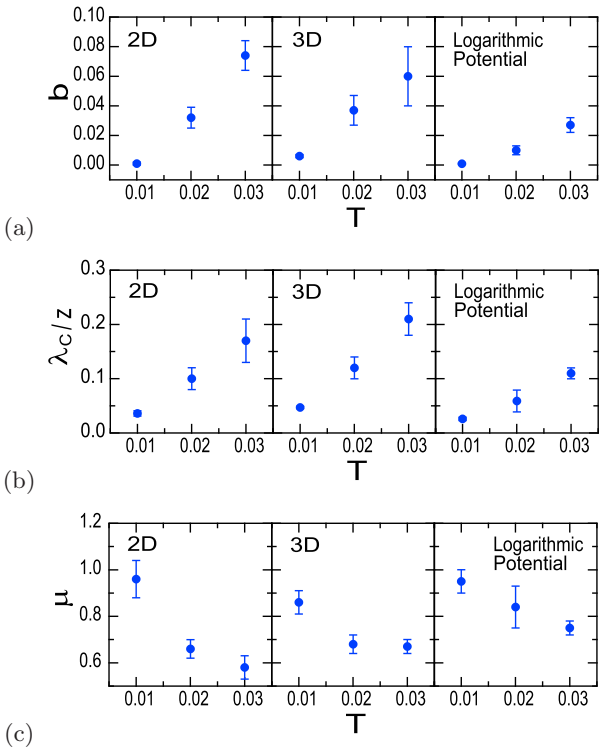

FIG. 10: Aging scaling exponents at $K = 1/2$ as functions of T for the Coulomb glass ($1/r$ interaction) in two (left panels) and three dimensions (center), and for the Bose glass (with logarithmic repulsion, right): (a) full aging scaling exponent b, Eq. (6) with $\mu = 1$; (b) autocorrelation decay exponent λ_C/z, Eq. (7); (c) subaging exponent μ, Eq. (6) with $b = 0$.

C. Coulomb / Bose Glass Aging Scaling Exponents

We collected data for the two-time density autocorrelation function for the Coulomb glass model in two (with $L = 16$, $N = 256$) and three dimensions ($L = 8$, $N = 512$), as well as for the two-dimensional Bose glass with essentially logarithmic repulsion ($L = 24$, $N = 576$) at various temperatures and filling fractions. We then determined the associated scaling exponents in the long-time aging regime following the procedures outlined in the previous subsection. (The resulting scaling plots can be found in Ref. [46].)

The thus obtained full-aging scaling exponents b and λ_C/z, see Eqs. (6) with $\mu = 1$ and (7), are compiled in Fig. 10(a) and (b) at half filling $K = 1/2$ as functions of the temperature T (see also Refs. [31, 32]). As one would expect, the non-equilibrium relaxation from the randomized initial state slows down drastically upon lowering the temperature, here clearly reflected in successively smaller values for b and λ_C/z as T is reduced from 0.03 to 0.01. Indeed, for even lower temperatures $T < 0.01$, our systems basically freeze in and we could not obtain statistically meaningful data for the ensuing extremely rare relaxation events. At $T = 0.01$, we find $b = 0.001 \pm 0.001$ for the two-dimensional Coulomb glass, see the left panel in Fig. 10(a), borderline consistent with the recently developed mean-field theory for aging relaxation in disordered electron glasses that predicts logarithmic scaling [33, 34, 36, 38]. However, in three dimensions we measure $b = 0.006 \pm 0.001$ at our lowest accessible temperature $T = 0.01$ (center panel), while for the two-dimensional Bose glass $b = 0.0009 \pm 0.0003$ (right panel). The associated autocorrelation to dynamic exponent ratios at $T = 0.01$ are $\lambda_C/z = 0.036 \pm 0.005$ (Coulomb glass, $d = 2$), $\lambda_C/z = 0.047 \pm 0.002$ (Coulomb glass, $d = 3$), and $\lambda_C/z = 0.026 \pm 0.003$ (Bose glass, $d = 2$), see Fig. 10(b). Note that relaxation processes in the Bose glass generically happen much slower as compared to the Coulomb glass (in $d = 2$ and $d = 3$ dimensions), as a consequence of the much shallower soft gap in the density of states, see Figs. 2(a) and 4(a).

Our corresponding results from the alternative subaging scaling analysis, Eq. 6 with $b = 0$, are plotted in Fig. 10(c). Note that the drastic slowing-down of the relaxation processes with reduced temperature now becomes apparent as a marked increase of the subaging scaling exponent μ, which almost approaches 1 for the two-dimensional Coulomb glass at $T = 0.01$. At this lowest temperature and half filling $K = 1/2$, our data yield $\mu = 0.96 \pm 0.008$ and $\mu = 0.86 \pm 0.05$ for the Coulomb glass in two and three dimensions, respectively, and $\mu = 0.9 \pm 0.0$ for the two-dimensional Bose glass.

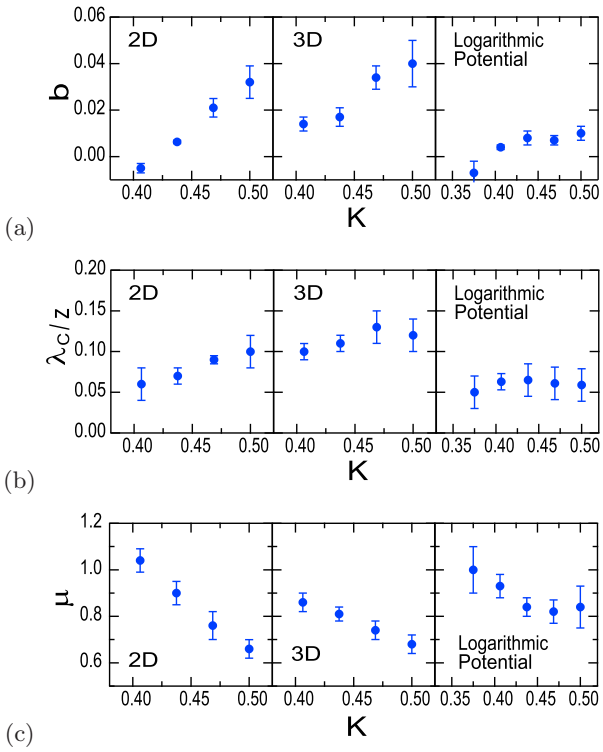

FIG. 11: Aging scaling exponents at $T = 0.02$ as functions of K for the Coulomb glass ($1/r$ interaction) in two (left panels) and three dimensions (center), and for the Bose glass (with logarithmic repulsion, right): (a) full aging scaling exponent b, Eq. (6) with $\mu = 1$; (b) autocorrelation decay exponent λ_C/z, Eq. (7); (c) subaging exponent μ, Eq. (6) with $b = 0$.

Intriguingly, our data reveal that the aging scaling exponents also depend on the total charge carrier density K. As evidenced in Fig. 11, the non-equilibrium relaxation processes from the initial high-temperature configurations proceed increasingly slower as the filling fraction K is tuned away from $K = 1/2$. These plots list our results measured at $T = 0.02$ for $K = 0.40625$, 0.4375, 0.46875, and $K = 0.5$ for the Coulomb glass model in two (left panels) and three dimensions (center panels), as well as in addition for $K = 0.375$ for the two-dimensional Bose glass system; but recall that owing to particle-hole symmetry the same data apply for both $K = 0.5 \pm k$ above and below half-filling. At the lowest filling fractions we investigated for the two-dimensional Coulomb and Bose glasses, we already obtain unphysical values $b < 0$ and correspondingly $\mu > 1$: These systems at $K = 0.40625$ and 0.375, respectively, are already frozen in on the time domain accessible to our Monte Carlo simulations. We are hence limited to the carrier density range $0.4 < K < 0.6$.

Within the full-aging scaling analysis, Figs. 11(a) and (b), it is apparent that the Bose glass exponents display a much weaker dependence on the filling fraction than is visible for either the two- or three-dimensional Coulomb glass. We tentatively attribute this observation to the considerably wider soft gap in the density of states that emerges for the logarithmic interaction potential as compared with the Coulomb $1/r$ repulsion, compare Figs. 2(a) and 4(a). In the long-time aging scaling regime, spatial rearrangements only redistribute energy levels deep inside this Coulomb gap, which attains a much more K-independent shape and still remains very shallow for the Bose glass in, e.g., the interval $|\epsilon - \mu_c| \leq 0.5$, for which the effects of modified filling fractions already become clearly discernible in the Coulomb glass. Remarkably, though, our data yield a noticeable dependence of the subaging scaling exponent μ even for the Bose glass with logarithmic interactions.

Consequently, the aging scaling exponents in the Coulomb and Bose glass appear to be non-universal, depending both on temperature and filling fraction, aside from dimensionality and the form of the long-range repulsive potential. Non-universal aging scaling has also been observed in other disordered systems, as for example the two-dimensional random-site [58] and random-bond [59, 60] Ising models or the three-dimensional Edwards-Anderson spin glass with a bimodal distribution of the coupling constants [60, 61], where some of the scaling exponents were found to depend on temperature and/or the disorder. Our present work therefore provides additional interesting examples of disordered systems that display non-universal aging exponents.

IV. SUMMARY AND CONCLUSIONS

We have carefully investigated non-equilibrium relaxation processes and aging scaling of the Coulomb glass model in two and three dimensions, and of the Bose glass system in two dimensions through Monte Carlo simulations at low temperatures. We confirm that the long-time dynamics in the α relaxation regime for the two-time autocorrelation function can be described by the simple general aging scaling form (6). We have employed either full-aging or subaging simplified scaling forms, and assess that neither version appears to provide substantially superior scaling collapse, although on physical grounds we tend to prefer full-aging scaling described by Eq. (6) with $\mu = 1$ and Eq. (7). The extracted aging scaling exponents depend on the filling fraction and temperature, in addition to dimensionality and form of the repulsive interaction potential, and are hence not universal. Moreover they follow a common trend: We observe that as either the temperature decreases or the charge carrier density deviates more from half-filling, the aging exponents reflect considerably slowed-down relaxation kinetics.

A series of recent studies [58, 60, 62] has shown that in disordered coarsening systems governed by a single length scale $L(t)$ one typically encounters rather complicated growth laws, characterized by a cross-over from a transient power-law growth to asymptotically logarithmic growth. Using this length $L(t)$ as variable in the aging scaling analysis reveals that the full aging scenario

prevails in these systems. It it an interesting question whether a similar cross-over between different growth regimes also exists in the Coulomb and Bose glasses, for which we would tentatively interpret $L(t)$ to describe the emerging spatial (anti-)correlations as the mutually repelling particles relax towards more energetically favorable sites. One way to extract a time-dependent length is through an analysis of the space-time correlation function. Computing this correlation function is a challenging task for our off-lattice model with long-range repulsive interactions. Because of the importance of this length in the non-equilibrium relaxation process, we plan to come back to this issue in the future.

Acknowledgments

This research is supported by the U.S. Department of Energy, Office of Basic Energy Sciences, Division of Materials Sciences and Engineering under Award DE-FG02-09ER46613.

[1] A. L. Efros and B. I. Shklovskii, J. Phys. C: Solid State Phys. **8**, L49 (1975).
[2] B. I. Shklovskii and A. L. Efros, *Electronic Properties of Doped Semiconductors* (Springer, New York, 1984).
[3] A. L. Efros and M. Pollak, *Electron-Electron Interactions in Disordered Systems* (North-Holland, Amsterdam, 1985).
[4] J. G. Massey and M. Lee, Phys. Rev. Lett. **75**, 4266 (1995).
[5] V. Yu. Butko, J. F. DiTusa, and P. W. Adams, Phys. Rev. Lett. **84**, 1543 (2000).
[6] G. Blatter, M. V. Feigel'man, V. B. Geshkenbein, A. I. Larkin, and V. M. Vinokur, Rev. Mod. Phys. **66**, 1125 (1994).
[7] I. F. Lyuksyutov, Europhys. Lett. **20**, 273 (1992).
[8] D. R. Nelson and V. M. Vinokur, Phys. Rev. Lett. **68**, 2398 (1992).
[9] D. R. Nelson and V. M. Vinokur, Phys. Rev. B **48**, 13060 (1993).
[10] U. C. Täuber, H. Dai, D. R. Nelson, and C. M. Lieber, Phys. Rev. Lett. **74**, 5132 (1995).
[11] U. C. Täuber and D. R. Nelson, Phys. Rev. B **52**, 16106 (1995).
[12] C. Wengel and U. C. Täuber, Phys. Rev. Lett. **78**, 4845 (1997).
[13] C. Wengel and U. C. Täuber, Phys. Rev. B **58**, 6565 (1998).
[14] J. H. Davies, P. A. Lee, and T. M. Rice, Phys. Rev. Lett. **49**, 758 (1982).
[15] M. Grünewald, B. Pohlmann, L. Schweitzer, and D. Würtz, J. Phys. C: Solid State Phys. **15**, L1153 (1982).
[16] J. H. Davies, P. A. Lee, and T. M. Rice, Phys. Rev. B **29**, 4260 (1984).
[17] E. I. Levin, V. L. Nguen, B. I. Shklovskii, and A. L. Efros, Sov. Phys. JETP **65**, 842 (1987).
[18] W. Xue and P. A. Lee, Phys. Rev. B **38**, 9093 (1988).
[19] A. Möbius, M. Richter, and B. Drittler, Phys. Rev. B **45**, 11568 (1992).
[20] E. R. Grannan and C. C. Yu, Phys. Rev. Lett. **71**, 3335 (1993).
[21] D. Menashe, O. Biham, B. D. Laikhtman, and A. L. Efros, EPL (Europhysics Letters) **52**, 94 (2000).
[22] D. Menashe, O. Biham, B. D. Laikhtman, and A. L. Efros, Phys. Rev. B **64**, 115209 (2001).
[23] M. Müller and S. Pankov, Phys. Rev. B **75**, 144201 (2007).
[24] B. Surer, H. G. Katzgraber, G. T. Zimanyi, B. A. Allgood, and G. Blatter, Phys. Rev. Lett. **102**, 067205 (2009).
[25] M. Goethe and M. Palassini, Phys. Rev. Lett. **103**, 045702 (2009).
[26] A. L. Efros, B. Skinner, and B. I. Shklovskii, Phys. Rev. B **84**, 064204 (2011).
[27] A. Pérez-Garrido, M. Ortuño, A. Díaz-Sánchez, and E. Cuevas, Phys. Rev. B **59**, 5328 (1999).
[28] C. C. Yu, Phys. Rev. Lett. **82**, 4074 (1999).
[29] A. Díaz-Sánchez and A. Pérez-Garrido, Eur. Phys. J. B **24**, 483 (2001).
[30] D. N. Tsigankov, E. Pazy, B. D. Laikhtman, and A. L. Efros, Phys. Rev. B **68**, 184205 (2003).
[31] D. R. Grempel, EPL (Europhysics Letters) **66**, 854 (2004).
[32] A. B. Kolton, D. R. Grempel, and D. Domínguez, Phys. Rev. B **71**, 024206 (2005).
[33] A. Amir, Y. Oreg, and Y. Imry, Phys. Rev. B **77**, 165207 (2008).
[34] A. Amir, Y. Oreg, and Y. Imry, Phys. Rev. Lett. **103**, 126403 (2009).
[35] M. Kirkengen and J. Bergli, Phys. Rev. B **79**, 075205 (2009).
[36] A. Amir, Y. Oreg, and Y. Imry, Phys. Rev. B **80**, 245214 (2009).
[37] M.T. Shimer, U.C. Täuber, and M. Pleimling, EPL (Europhys. Lett.) **91**, 67005 (2010).
[38] A. Amir, Y. Oreg, and Y. Imry, Annual Rev. Condens. Matter Phys. **2**, 235 (2011).
[39] A. Amir, S. Borini, Y. Oreg, and Y. Imry, Phys. Rev. Lett. **107**, 186407 (2011).
[40] Y. Meroz, Y. Oreg, and Y. Imry, EPL (Europhys. Lett.) **105**, 37010 (2014).
[41] A. Amir, e-print `arXiv:1403.3098` (2014).
[42] J. Jaroszyński and D. Popović, Phys. Rev. Lett. **99**, 046405 (2007).
[43] J. Jaroszyński and D. Popović, Phys. Rev. Lett. **99**, 216401 (2007).
[44] M. Henkel, M. Pleimling, and R. Sanctuary (eds.), *Ageing and the Glass Transition*, Lecture Notes in Physics **716** (Springer, Berlin, 2007).
[45] M. Henkel and M. Pleimling, *Non-Equilibrium Phase Transitions, Vol. 2: Ageing and Dynamical Scaling Far From Equilibrium* (Springer, Dordrecht, 2010).
[46] M.T. Shimer, *Nonequilibrium Relaxation and Aging Scaling Properties of the Coulomb Glass and Bose Glass*, Ph.D. dissertation, Virginia Tech (2011); available at

http://scholar.lib.vt.edu/theses/available/etd-09092011-104434/ .
[47] W. Götze and L. Sjogren, Rep. Prog. Phys. **55**, 241 (1992).
[48] C. Godrèche and J. M. Luck, J. Phys. A: Math. Gen. **33**, 1151 (2000).
[49] E. Lippiello and M. Zannetti, Phys. Rev. E **61**, 3369 (2000).
[50] H. K. Janssen, B. Schaub, and B. Schmittmann, Z. Phys. B **73**, 539 (1989).
[51] P. Calabrese and A. Gambassi, J. Phys. A: Math. Theor. **38**, R133 (2005).
[52] A. Coniglio and M. Zannetti, Phys. Rev. B **42**, 6873 (1990).
[53] G. Biroli, J. Stat. Mech., P05014 (2005).
[54] S. A. Cannas, D. .A. Stariolo, and F. A. Tamarit, Physica A **294**, 362 (2001).
[55] F. Baumann, S. B. Dutta, and M. Henkel, J. Phys. A: Math. Gen. **40**, 7839 (2007).
[56] S. B. Dutta, J. Phys. A: Math. Gen. **41**, 395002 (2008).
[57] S. M. Bhattacharjee and F. Seno, J. Phys. A: Math. Gen. **34**, 6375 (2001).
[58] H. Park and M. Pleimling, Phys. Rev. B **82**, 144406 (2010).
[59] M. Henkel and M. Pleimling, Phys. Rev. B **78**, 224419 (2008).
[60] H. Park and M. Pleimling, Eur. Phys. J B **85**, 300 (2012).
[61] J. Kisker, L. Santen, M. Schreckenberg, and H. Rieger, Phys. Rev. B **53**, 6418 (1996).
[62] F. Corberi, E. Lippiello, A. Mukherjee, S. Puri, and M. Zannetti, Phys. Rev. E **85**, 021141 (2012).